J Mater Sci (2012) 47:6086–6094
DOI 10.1007/s10853-012-6523-y

Preparation of Ag–Fe-decorated single-walled carbon nanotubes by arc discharge and their antibacterial effect

Xing Liu · Liming Yu · Feng Liu · Leimei Sheng · Kang An · Hongxia Chen · Xinluo Zhao

Received: 16 February 2012 / Accepted: 20 April 2012 / Published online: 5 May 2012

Abstract A simple one-step approach for the preparation of Ag–Fe-decorated single-walled carbon nanotubes (Ag–Fe/SWCNTs) by DC hydrogen arc discharge is presented in this article. The growth of SWCNTs and the attachment of Ag and Fe nanoparticles to the SWCNTs occur simultaneously during the arc discharge evaporation process. It has been confirmed that the Ag and Fe nanoparticles in the diameter range of 1–10 nm are well dispersed and tightly attached to the outer surfaces of SWCNTs. The as-grown Ag–Fe/SWCNTs have been purified by high-temperature hydrogen treatment to remove amorphous carbon and carbon shells. Antibacterial tests show that the antibacterial activity of the purified Ag–Fe/SWCNT hybrid nanoparticles is excellent against *Escherichia coli*. The percentage of the *E. coli* killed by 100 μg/ml Ag–Fe/SWCNTs can reach up to 85.1 % at a short residence time of 2 h, suggesting that the purified Ag–Fe/SWCNTs may have potential antibacterial applications.

Electronic supplementary material The online version of this article (doi:10.1007/s10853-012-6523-y) contains supplementary material, which is available to authorized users.

X. Liu · L. Yu (✉) · L. Sheng · K. An · X. Zhao (✉)
Department of Physics, and Institute of Low-dimensional Carbons and Device Physics, Shanghai University, Shanghai 200444, China
e-mail: lmyu@shu.edu.cn

X. Zhao
e-mail: xlzhao@shu.edu.cn

F. Liu · H. Chen
School of Life Sciences, Shanghai University, Shanghai 200444, China

Introduction

Single-walled carbon nanotubes (SWCNTs) have attracted tremendous attention in recent years because of their remarkable physical, chemical, and mechanical properties. With all atoms remaining exposed on the surface, SWCNTs have ultrahigh specific surface area. They can easily form a two-dimensional network because of their high length-to-diameter ratio. These allow SWCNTs and their networks to act as extraordinary support materials. Multiple molecules and nanoparticles have been used to decorate SWCNTs to form new composites, and these composites display interesting properties for various applications [1].

In recent years, many researchers have tried to explore the potential biological applications of SWCNTs, motivated by their unique structure as well as outstanding physical properties. CNT-based drug delivery has shown a great future in various biological experiments. Sensitive, multiplexed biosensors based on SWCNT show good prospects for the detection of early stage cancer. Biological imaging using SWCNTs is also realized because of their intrinsic optical properties [2, 3]. Particularly, silver-decorated carbon nanotubes (Ag/CNTs) have attracted a great deal of attention. Many studies have reported on the potential applications of Ag/CNTs as catalysts [4], conductive materials [5], biosensors [6–8], and antibacterial materials [9].

Silver is generally known as a highly safe material with a wide antibacterial spectrum. Ag nanoparticles are potential catalysts for H_2O_2 reduction [10], hydrazine oxidation [11], and they exhibit antimicrobial properties against kinds of bacterial pathogens [12, 13]. They are under increased investigation as supplemental bactericides to antibiotics since more and more bacteria have become

drug-resistant because of the abuse of antibiotic. The CNTs have also been found to have antibacterial activities, and SWCNTs are superior to multi-walled carbon nanotubes (MWCNTs) [14, 15]. The bacterial cell membrane is damaged through direct contact with SWCNTs leading to the cell death. Liu et al. [16] have found that SWCNT networks are developed on the cell surface and destroy the bacterial envelopes by the leakage of the intracellular contents. The Ag-decorated SWCNTs show a higher antibacterial activity than either of them alone [9].

Up to now, Ag/CNTs have been prepared by several methods, including electroless deposition [17], sonochemical technique [9], in situ reduction [18], and aerosol process [19]. Generally, the production of CNTs and the attachment of Ag nanoparticles on CNTs are done separately, involving complicated procedures. Additionally, the attachment of metal nanoparticles is usually preceded by the surface modification process of CNTs via surfactants or acid etching, introducing impurities or doing damage to the CNT walls.

In the present study, a simple one-step preparation process of hydrogen DC arc discharge was used to generate Ag–Fe-decorated SWCNTs (Ag–Fe/SWCNTs). The growth of SWCNTs and the attachment of Ag and Fe nanoparticles to SWCNTs occur simultaneously during the arc discharge evaporation process. Then, impurities of amorphous carbon and carbon shells were removed by the H_2-800 °C treatment. The antibacterial activity of purified Ag–Fe/SWCNTs against *E. coli* was also evaluated.

Experimental

Fabrication of carbon electrodes

The carbon anode was made by mixing carbon, Fe (<10 μm), and Ag powders (0.6–2 micron) together to form a cylinder with a diameter of 10 mm. The carbon powder was obtained by mixing petroleum coke (200 mesh) and pitch coke (~1 mm) in a ratio of 1:1, and ball-milling for 24 h. The Fe powders in the anode were used as the catalyst to produce SWCNTs. The ratios of Fe and Ag powders in the anode were 1.0 and 0.5 at%, respectively. Then the cylinder was annealed at high temperatures in Ar gas to remove tar oil and other impurities. Four temperatures (900, 1,200, 1,400, and 1,600 °C) were tried to determine the optimal treatment temperature of the Fe–Ag containing carbon anode. The cathode was a pure carbon electrode without metal in it.

Preparation of Ag–Fe/SWCNTs by arc discharge

Ag–Fe/SWCNTs were prepared by DC hydrogen arc discharge method. A DC arc discharge was generated between two horizontally installed electrodes by applying 80 A in the mixed atmosphere of H_2 and Ar (4:6/v:v) at a total pressure of 200 Torr. The distances of the anode and the cathode were maintained at about 2 mm by a step motor. During the arc discharge evaporation, SWCNTs were generated in the presence of Fe catalyst, and Ag nanoparticles loaded on the surface of SWCNTs. The loading of Ag nanoparticles and the growth of SWCNTs occurred almost at the same time. Fe-decorated SWCNTs (Fe/SWCNTs) were also prepared for comparison by the same method using the 1,600 °C-treated and only Fe-contained carbon anode.

Purification of Ag–Fe/SWCNTs

The as-grown Ag–Fe/SWCNTs contain impurities such as amorphous carbon and carbon shells, and most of the Ag and Fe nanoparticles are encapsulated in them. The as-grown Ag–Fe/SWCNTs were treated at 800 °C in the mixed atmosphere of H_2 and Ar (2:8/v:v) with a total flow rate of 100 sccm for 1 h. The amorphous carbon coexisting with SWCNTs and the carbon shells encapsulating Ag and Fe nanoparticles were converted to CH_4 during the high-temperature H_2 treatment process, while SWCNTs survived [20]. As grown Fe/SWCNTs were purified by H_2-800 °C-1 h treatment, and pure SWCNTs were obtained by further acid treatment.

Characterization

The as-grown and purified Ag–Fe/SWCNTs were characterized by a laser micro-Raman spectrometer (Renishaw, invia plus) with an excitation wavelength of 514 nm. The morphology of the nanotubes and the metal nanoparticles were observed by scanning electron microscope (SEM) (FE-SEM, JEOL JSM-6700F), transmission electron microscope (TEM) (JEOL JEM-200CX), and high-resolution TEM (HRTEM) (Tecnai G2 F20 S-Twin). The existent elements in the Ag–Fe/SWCNTs were evaluated by an energy dispersive spectroscopy analyzer (EDS, Oxford Inca). The structures of the samples were characterized by X-ray diffraction (XRD) patterns (Rigaku Corporation DLMAX-2200) in the 2θ range from 25° to 85° at a scanning speed of 1° min^{-1}.

Antibacterial tests

The antibacterial activities of pure SWCNTs, purified Fe/SWCNTs, and purified Ag–Fe/SWCNTs were evaluated against *Escherichia coli* by a culture-colony counting method. Gram-negative *E. coli* was chosen because gram-negative bacteria are responsible for more than 80 % of infections. All glass wares and materials were sterilized in an autoclave at 121 °C for 20 min before the experiments.

E. coli was cultivated in a liquid Luria–Bertani (LB) medium and then incubated with a shaking incubator for 24 h (37 °C, 200 rpm). In the antibacterial test of Ag–Fe/SWCNTs, Ag–Fe/SWCNT suspensions at different concentrations were prepared by adding the H_2-800 °C-1-h-purified Ag–Fe/SWCNT powders into ultra-pure water and tip-sonicated (200 W) for 30 min. Then 1 ml of the sterilized Ag–Fe/SWCNT suspension (10 μg/ml, or 100 μg/ml) was inoculated with 10 μl of the 24-h cultured *E. coli* suspension. The ultra-pure water inoculated with the *E. coli* suspension without Ag–Fe/SWCNTs in it was taken as the control group. After mixing them well, the resultant suspensions were incubated with a shaking incubator for 2 h (37 °C, 200 rpm). Then they were diluted 1,000 times, and 50 μl of the dilutions were spread on each LB agar plate and incubated at 37 °C for 16 h. Each healthy cell on the LB agar plate multiplies and generated a colony of bacteria after incubation, and these colonies can be easily seen by the naked eye. The number of colonies on the plates was counted. For each group (*E. coli*/ultra-pure water, *E. coli*/10 μg/ml Ag–Fe/SWCNTs, and *E. coli*/100 μg/ml Ag–Fe/SWCNTs), three plates were made, and the average value was obtained. The percent kill of *E. coli* by purified Ag–Fe/SWCNTs was calculated as a percentage of the colony-forming units obtained from the control group. The antibacterial tests of SWCNTs and Fe/SWCNTs were conducted just like the test method of Ag–Fe/SWCNTs. However, only one concentration (100 μg/ml) was tested.

Results and discussion

Characteristics of Ag–Fe/SWCNTs

Figure 1a shows a typical SEM image of the as-grown Ag–Fe/SWCNTs. The SWCNT bundles formed into a crisscross network, and the bright spots are metal nanoparticles. The EDS result confirms that Ag and Fe coexist in the sample (Fig. 1b). In addition to C, Ag, and Fe peaks, a sulfur (S) peak appears because some sulfur exists in the raw carbon powders. Figure 1c shows the Raman spectra of the as-grown Ag–Fe/SWCNTs generated from carbon anodes treated at 900, 1,200, 1,400, and 1,600 °C. The intensity ratio of the D- and G-bands (I_D/I_G) can represent the crystallinity and the relative amount of amorphous carbon in the SWCNT samples. The lower the I_D/I_G value,

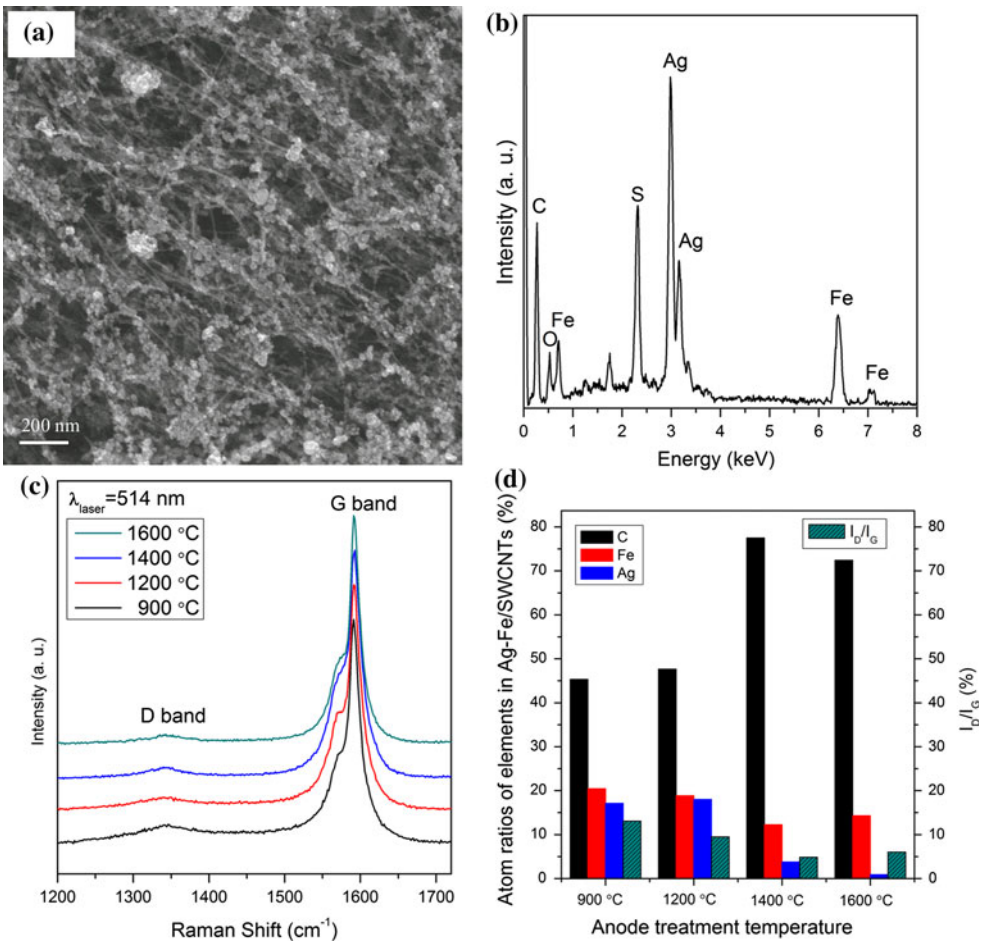

Fig. 1 **a** SEM image of the as-grown Ag–Fe/SWCNTs; **b** EDS result of an as-grown Ag–Fe/SWCNT sample; **c** Raman spectra of the as-grown Ag–Fe/SWCNTs generated from carbon anodes treated at 900, 1,200, 1,400, and 1,600 °C, respectively; and **d** histogram for the element atom ratios and I_D/I_G values of the as-grown Ag–Fe/SWCNTs. The Raman spectra are normalized to the intensity of the G-band. The atom ratios of carbon, Fe and Ag in the as-grown Ag–Fe/SWCNTs, are obtained from the EDS results. The I_D/I_G values are obtained from the Raman spectra

the higher the purity of the SWCNT sample. Figure 1d is the histogram for the element atom ratios and I_D/I_G values of the as-grown Ag–Fe/SWCNTs generated from carbon anodes treated at different temperatures. Zhao et al. [21] have pointed out that the optimal treatment temperature is 1,600 °C for carbon anode containing only Fe catalyst. However, the melting point of Ag is only 961.8 °C, which is much lower than that of Fe (1,535 °C). The experimental results show that the amount of Ag in the as-grown Ag–Fe/SWCNTs becomes very low when the anodes are treated at 1,400 or 1,600 °C. Ag does not lose when the anodes are treated at 900 and 1,200 °C. It is also seen from Fig. 1d that the I_D/I_G value of the as-grown Ag–Fe/SWCNTs generated from carbon anodes treated at 1,200 °C is lower than that at 900 °C. In brief, the amount of Ag will reduce greatly when the anode's treatment temperature is too high, but the quality of SWCNTs will get worse when the temperature is too low. Hence, we finally chose 1,200 °C as the optimal treatment temperature of the carbon anode for the following experiments.

It is interesting to find that Ag does not lose when the anodes are treated at 1,200 °C. One possible mechanism is that Ag is enwrapped by carbon grains during the densification process of the anodes. During the thermal treatment process, densification of the anodes occurs. The point contact of carbon grains slowly changed to surface contact, leading Ag and Fe particles trapped in the carbon grains. Although Ag particles have melted at 1,200 °C, they could not evaporate. When the annealing temperature increases to 1,300°C (1,250–1,500 °C), more severe interface movements and interactions occur, and cause many new cracks. In this case, Ag begins to evaporate. When the annealing temperature is close to 1,600 °C, Fe begins to react with carbon and forms Fe–C solid solution [21], while Ag evaporates more quickly, and finally disappears.

The as-grown Ag–Fe/SWCNTs contain impurities such as amorphous carbon coexisting with SWCNTs and carbon shells encapsulating Ag and Fe nanoparticles. Here, high temperature hydrogen treatment was used to purify the as-grown Ag–Fe/SWCNT samples. Figure 2 shows the Raman spectra of the as-grown and H_2-800 °C purified Ag–Fe/SWCNTs. The diameters of SWCNTs, d_t, can be obtained by the formula

$$\omega_{RBM} = 234/d_t + 10\,\mathrm{cm}^{-1},$$

where $\omega_{RBM}(\mathrm{cm}^{-1})$ is the wavenumber of the radial breathing mode (RBM) appearing in the Raman spectrum [22]. There are several RBM peaks appearing in the range of 110–180 cm^{-1}, which correspond to a diameter range of 1.4–2.3 nm. Hydrogen treatment did not significantly change the size distribution of the SWCNTs.

The diameters of the SWCNTs generated by Ag–Fe contained carbon anodes are larger than those generated by

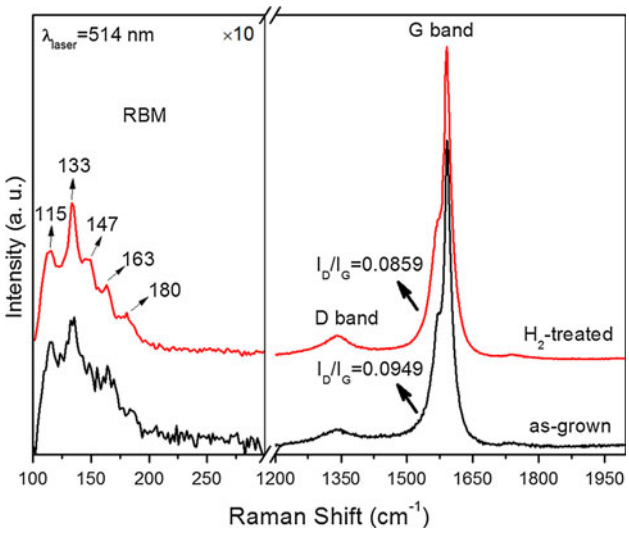

Fig. 2 Raman spectra of the as-grown and purified Ag–Fe/SWCNTs at an excitation wavelength of 514 nm. The Raman spectra have been normalized to the intensity of the G-band

pure-Fe-catalyzed ones. The reason might be that the existent Ag in the anode hinders the growth of small diameter tubes. The lower treatment temperature of the anode may also be one reason. Compared with the as-grown Ag–Fe/SWCNTs, the I_D/I_G value of the H_2-800 °C purified sample decreased from 0.0949 to 0.0859, indicating a higher purity.

As is well known, the melting temperature of nanoparticles depends on their sizes. For substrate-supported nanoparticles with relatively free surface, the melting temperature decreases with the decreasing particle sizes [23]. The melting point of bulk Ag is 961.8 °C. For particles of spherical geometry with diameter d, the melting point can be calculated from the formula [24]

$$\frac{T_m}{T_{mb}} = 1 - \frac{\beta}{d},$$

where T_m represents the melting temperature of the nanoparticles, T_{mb} is the bulk melting temperature, and β is the material constant. According to the formula, the melting points of Ag nanoparticles with diameters of 10, 5, and 2 nm are 841, 722, and 365 °C, respectively. For Fe with the same sizes, the melting points are 1,365, 1,195, and 683 °C, respectively. Hence, Ag nanoparticles may melt and aggregate to larger particles during the H_2-800 °C treatment.

Figure 3 shows the XRD patterns of the as-grown, H_2-800 °C-0.5-h-purified, and H_2-800 °C-1-h-purified Ag–Fe/SWCNTs. According to the JCPDS card No. 04-0783, the diffraction peaks at $2\theta = 38.114°$, 44.298°, 64.441°, 77.395°, and 81.538° are indexed to Ag (111), Ag (200), Ag (220), Ag (311), and Ag(222), respectively. The Ag metal crystal has a face-centered cubic symmetry. The

corresponding peaks become very sharp after annealing in H_2, indicating the growth of the grain sizes. Taking the Ag (111) peak, for example, the peak height of the as-grown sample is only 334, and it increases to 946 and 2,582 after 0.5-h and 1-h annealing, respectively. It can be concluded that the aggregation of Ag nanoparticles occurs during the H_2-800 °C treatment, and the longer the treating time, the larger the aggregation degree.

According to the JCPDS card No. 85-1410, the corresponding diffraction peaks of Fe (110), Fe (200), and Fe (211) are at $2\theta = 44.352°$, 64.526°, and 81.654°, respectively. They almost overlap with the peaks of Ag (200) at 44.298°, Ag (220) at 64.441°, and Ag (222) at 81.538°. Some Fe_3O_4 peaks appear after H_2 treatment according to the JCPDS card No. 89-2355. It is because carbon impurities that encapsulate the metal nanoparticles are removed by H_2 treatment, and Fe nanoparticles are oxidized by oxygen when the Ag–Fe/SWCNTs are taken out in air. The Ag nanoparticles are not oxidized according to the XRD results.

For the H_2-treated samples, several additional small peaks appear in the 2θ range of 28°-46°. They are generated from silver sulfide (Ag_2S) according to the JCPDS card No. 14-0072. It is because a certain amount of sulfur is remained in the samples and reacts with Ag. Ag_2S does not exist in the as-grown Ag–Fe/SWCNTs because the arc temperature is too high to produce Ag_2S, and the Ag nanoparticles are encapsulated in carbon shells. After H_2 treatment, most of carbon shells are removed, and some Ag nanoparticles react with S at relatively low temperatures to form Ag_2S.

Figure 4a–c shows the TEM images of Ag–Fe/SWCNTs before and after purification. The dark spots on the surface of SWCNT bundles are metal nanoparticles. For the as-grown sample, the metal nanoparticles are dispersed homogeneously, but they are surrounded or encapsulated in amorphous carbon and carbon shells (Fig. 4a). After H_2-800 °C treatment for an hour, most carbon impurities are removed (Fig. 4b–c). It can be seen from the TEM and HRTEM images that most Ag and Fe nanoparticles are in the diameter range of 1–10 nm, while some nanoparticles aggregate to several tens of nanometers (Fig. 4c). The spherical big-sized nanoparticles are thought to be Ag while the square big ones are thought to be Fe oxides. The aggregation is consistent with the XRD results. The arrowed large particle in Fig. 4c is confirmed to be Ag by the EDS result (Fig. 4d). The TEM images of pure SWCNTs and purified Fe/SWCNTs can be seen in our previously study [20].

Tylazin et al. [25] have found that the reaction of SWCNTs with hydrogen gas at 550 °C and at hydrogen pressure of 50 bar (5 MPa) can successfully remove all carbon coatings enclosing Fe particles in pristine samples. The H_2-treatment temperature may be decreased at higher pressure to reduce the aggregation of Ag nanoparticles. Figure 4e–f show the HRTEM images of H_2-purified Ag–Fe/SWCNTs. The arrows in Fig. 4e show SWCNTs with different diameters. Figure 4f demonstrates that Ag and Fe nanoparticles are dispersed on the surfaces of CNT bundles. The upper inset in Fig. 4f is a local, magnified image (marked by the upper black arrow) showing a Ag nanoparticle with a lattice spacing of 0.236 nm which is close to that of Ag (111). Similarly, the nanoparticle shown in the lower inset of Fig. 4f is Fe (110) with a lattice spacing of 0.204 nm. The metal nanoparticles are tightly attached to the side walls of SWCNTs by graphene sheets. This ensures that the metal nanoparticles cannot easily move to other parts of the tubes or exfoliate from them, showing a good stability.

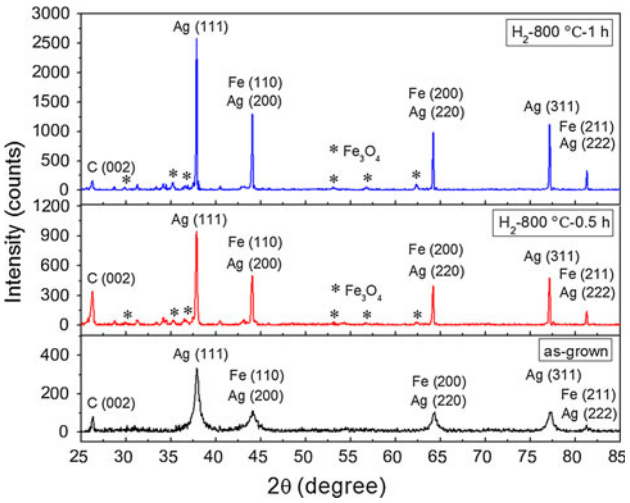

Fig. 3 XRD patterns of the as-grown, H_2-800 °C-0.5-h-purified, and H_2-800 °C-1-h-purified Ag–Fe/SWCNTs

Antibacterial behavior of Ag–Fe/SWCNTs

Escherichia coli is usually used as a model bacterial system for various antibacterial testing programs. The antibacterial efficacies of purified Ag–Fe/SWCNTs against *E. coli* for 2 h are shown in Fig. 5. Figure 5a shows the control group. Figure 5b and c shows the 10 μg/ml and 100 μg/ml Ag–Fe/SWCNT groups, respectively. Compared with the control group, the counts of forming bacterial colonies reduce greatly. This indicates that the growth of the *E. coli* is inhibited in the suspensions containing purified Ag–Fe/SWCNTs. The average percent kill of *E. coli* by the 10 μg/ml Ag–Fe/SWCNT sample is 71.4 %, while that by the 100 μg/ml Ag–Fe/SWCNT sample reaches to 85.1 % (Fig. 5d). The average percent kill of *E. coli* by the 100 μg/ml SWCNT and Fe/SWCNT samples are 21.6 and 18.9 %, respectively (Fig. S1). The results indicate a strong

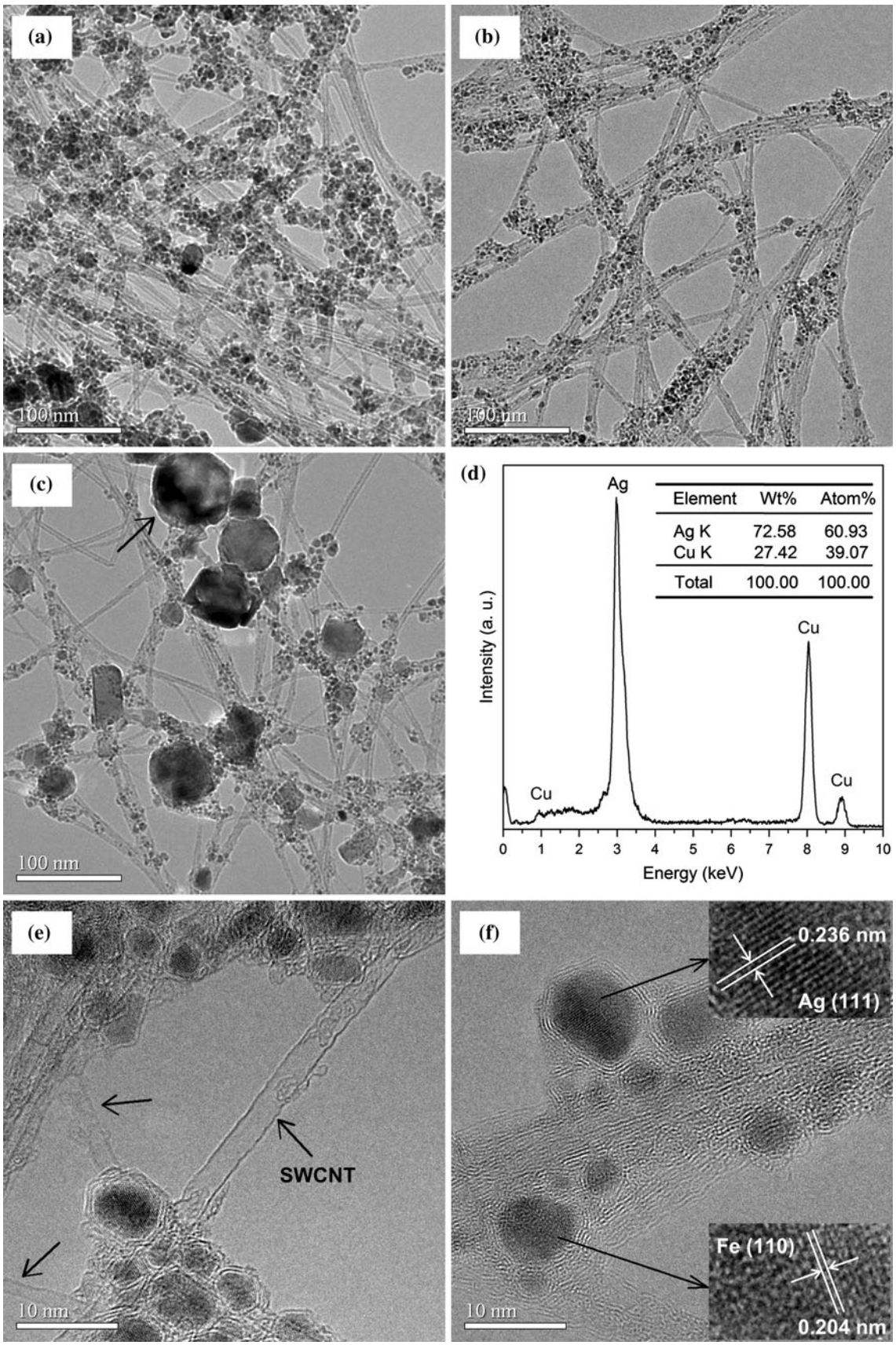
(a)
100 nm
(b)
100 nm
(c)
100 nm
(d)
Ag
Cu
Cu
Cu
Element Wt% Atom%
Ag K 72.58 60.93
Cu K 27.42 39.07
Total 100.00 100.00
Intensity (a. u.)
0 1 2 3 4 5 6 7 8 9 10
Energy (keV)
(e)
SWCNT
10 nm
(f)
0.236 nm
Ag (111)
Fe (110)
0.204 nm
10 nm

◀ **Fig. 4** **a** TEM image of the as-grown Ag–Fe/SWCNTs; **b**, **c** TEM images of the H_2-800 °C-1-h-purified Ag–Fe/SWCNTs; **d** EDS result of the particle marked in **c** by an arrow; and **e**, **f** HRTEM images of the purified Ag–Fe/SWCNTs. The insets are local, magnified images arrowed in **f**, representing the Ag and Fe nanoparticles, respectively

antibacterial effect of the purified Ag–Fe/SWCNT nanoparticles. The percent kill of *E. coli* can be improved by lengthening the exposure time of *E. coli* in the Ag–Fe/SWCNT suspensions.

The *E. coli* are killed because Ag ions are released in the Ag–Fe/SWCNT suspensions and exhibit strong antibacterial activity. The antibacterial mechanism of silver ions against *E. coli* is that silver ions can adsorb the protein on the surface of the bacterial membrane, interact with thiol groups in protein, and inhibit the replication abilities of the DNA, and finally lead to the death of bacteria [26]. *E. coli* in the suspensions may also collide with numerous Ag–Fe/SWCNTs in solution. The bacterial cell membrane can be damaged through direct contact with SWCNTs and Ag nanoparticles, which leads to the cell death. The antibacterial effect of SWCNTs has again been proved by our experiment. The dramatic improvement of Ag–Fe/SWCNTs (85.1 %) compared with pure SWCNTs (21.6 %) and Fe/SWCNTs (18.9 %) indicates that Ag plays the major role in killing the *E. coli*. The slight decrease of the percent kill of Fe/SWCNTs compared with SWCNTs can be ascribed to the relatively less amount of SWCNTs in the Fe/SWCNT sample than that in the SWCNT sample. The Fe nanoparticles and their oxides are not bio-compatible, and they also help in decreasing the viability of *E. coli* to a

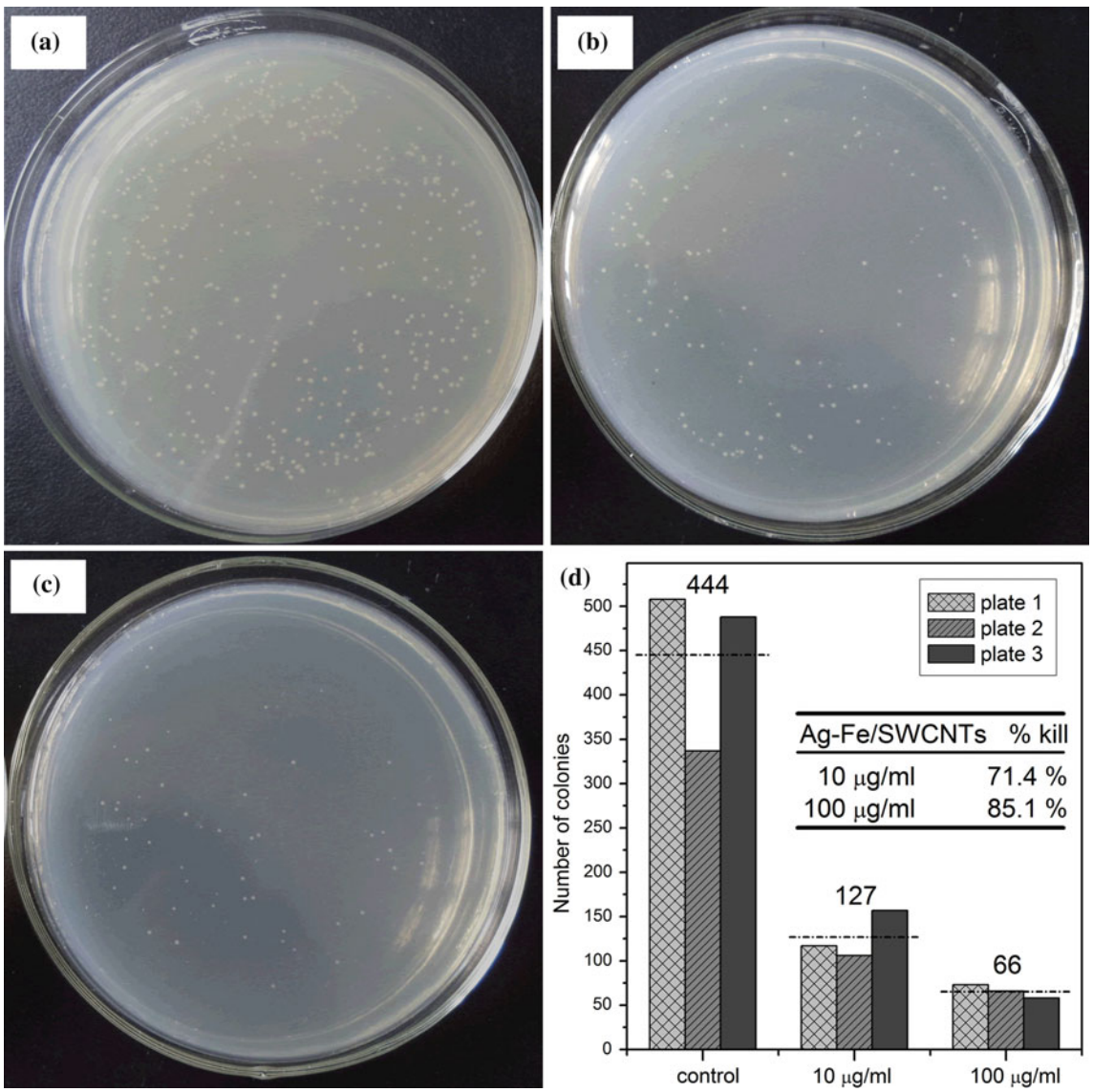

Fig. 5 Antibacterial tests of H_2-800 °C-1-h-purified Ag–Fe/SWCNTs. Photographs of LB agar plates inoculated with **a** *E. coli*/ultra-pure water, **b** *E. coli*/10 μg/ml Ag–Fe/SWCNTs, and **c** *E. coli*/100 μg/ml Ag–Fe/SWCNTs; and **d** histogram for the test results

certain extent. A correlation between increasing Fe catalyst amount and decreasing cell viability has been observed [27]. However, for the samples of the same weight, the amount of SWCNTs in the Fe/SWCNTs is much less than that in the pure SWCNTs, which weakens the antibacterial effect of SWCNTs. The slight decrease of percent kill of Fe/SWCNTs compared with pure SWCNTs indicates a higher antibacterial activity of SWCNTs than Fe nanoparticles and their oxides.

The one-step preparation of Ag–Fe/SWCNTs by the arc discharge method did not bring impurities such as various surfactants or introduce damage to the SWCNT side walls. Hence, the SWCNTs have a high crystallinity, which is one reason for the significant antibacterial effects of the Ag–Fe/SWCNTs. Ag and Fe nanoparticles are attached to the side walls of SWCNTs during the growth of the nanotubes, and they exist both inside and outside the tube bundles, permitting the Ag–Fe/SWCNTs to have a higher loading ratio of Ag nanoparticles compared with Ag/CNTs synthesized by two-step or multi-step methods. The embedded Ag nanoparticles also release Ag ions through the apertures of the SWCNT bundles, increasing the concentration of Ag ions in the suspensions. The Ag–Fe/SWCNTs prepared by the one-step DC arc discharge method are also more stable. The Ag and Fe nanoparticles are tightly attached by graphene sheets, showing a more steady structure than Ag/CNTs produced by chemical methods. The small diameters (1–10 nm) of most Ag and Fe nanoparticles enable them to own high specific surface area. This would also enhance the antibacterial activity of the metal nanoparticles. The excellent antibacterial activity of purified Ag–Fe/SWCNTs is a result of the combined actions of Ag ions/Ag nanoparticles, SWCNTs, and Fe nanoparticles/Fe oxides.

In this study, the *E. coli* are killed in the Ag–Fe/SWCNT solution; however, the antibacterial effect may be greatly enhanced by means of Ag–Fe/SWCNT-based filters because the direct physical piecing acts as the dominant factor for the antibacterial mechanism under filtration conditions and more cells will be killed [16, 19]. The more close contacts between Ag–Fe/SWCNT network and cells during the filtration process may also enhance the kill ratio, which requires further investigation.

Conclusions

In summary, we have demonstrated that Ag–Fe/SWCNTs can be prepared by means of a simple one-step DC hydrogen arc discharge method. The SWCNTs prepared by this method have a high crystallinity. Ag and Fe nanoparticles are uniformly dispersed and tightly attached to the surface of SWCNTs. Amorphous carbon and carbon shells were removed by H_2-800 °C treatment. The excellent crystallinity of the SWCNTs, the high loading ratio of Ag nanoparticles on SWCNTs, and the large specific surface area of Ag and Fe nanoparticles make purified Ag–Fe/SWCNTs exhibit excellent antibacterial activity against *E. coli*. These results suggest that purified Ag–Fe/SWCNTs have potential applications in the biological field such as biosensors, biofilters, and other antibacterial materials.

Acknowledgements Financial support from the National Natural Science Foundation of China (Grant No. 10974131) and Shanghai University-Solar Enertech Research&Development Joint Laboratory is gratefully acknowledged.

References

1. Georgakilas V, Gournisb D, Tzitziosa V, Pasquato L, Guldie DM, Prato M (2007) J Mater Chem 17:2679
2. Liu Z, Tabakman S, Welsher K, Dai HJ (2009) Nano Res 2:85
3. Liu Z, Sun XM, Nakayama-Ratchford N, Dai HJ (2007) ACS Nano 1:50
4. Yang GW, Gao GY, Wang C, Xu CL, Li HL (2008) Carbon 46:747
5. Ma PC, Tang BZ, Kim JK (2008) Carbon 46:1497
6. Chen YC, Young RJ, Macpherson JV, Wilson NR (2007) J Phys Chem C 111:16167
7. Sahoo S, Husale S, Karna S, Nayak SK, Ajayan PM (2011) J Am Chem Soc 133:4005
8. Hu HB, Wang ZH, Pan L, Zhao SP, Zhu SY (2010) J Phys Chem C 114:7738
9. Rangari VK, Mohammad GM, Jeelani S, Hundley A, Vig K, Singh SR, Pillai S (2010) Nanotechnology 21:5102
10. Lu WB, Chang GH, Luo YL, Liao F, Sun XP (2011) J Mater Sci 46:5260. doi:10.1007/s10853-011-5464-1
11. Hosseini M, Momeni MM (2010) J Mater Sci 45:3304. doi:10.1007/s10853-010-4347-1
12. Niu A, Han YJ, Wu J, Yu N, Xu Q (2010) J Phys Chem C 114:12728
13. Zhang Y, Zhong SL, Zhang MS, Lin YC (2009) J Mater Sci 44:457. doi:10.1007/s10853-008-3129-5
14. Kang S, Pinault M, Pfefferle LD, Elimelech M (2007) Langmuir 23:8670
15. Kang S, Herzberg M, Rodrigues DF, Elimelech M (2008) Langmuir 24:6409
16. Liu SB, Ng AK, Xu R, Wei J, Tan CM, Yang YH, Chen Y (2010) Nanoscale 2:2744
17. Yan DS, Wang F, Zhao YB, Liu JJ, Wang JJ, Zhang LH, Park KC, Endo M (2009) Mater Lett 63:171
18. Yuan W, Jiang GH, Che JF, Qi XB, Xu R, Chang MW, Chen Y, Lim SY, Dai J, Chan-Park MB (2008) J Phys Chem C 112:18754
19. Jung JH, Hwang GB, Lee JE, Bae GN (2011) Langmuir 27:10256
20. Sheng LM, Shi L, An K, Yu LM, Ando Y, Zhao XL (2011) Chem Phys Lett 502:101
21. Zhao XL, Kadoya T, Ikeda T, Suzuki T, Inoue S, Ohkohchi M, Takimoto Y, Ando Y (2007) Diamond Relat Mater 16:1101
22. Kuzmany H, Plank W, Hulman M, Kramberger Ch, Gruneis A, Pichler Th, Peterlik H, Kataura H, Achiba Y (2001) Eur Phys J B 22:307
23. Goldstein AN (1996) Appl Phys A Mater Sci Process 62:33
24. Nanda KK, Sahu SN, Behera SN (2002) Phys Rev 66:013208

25. Talyzin AV, Luzan S, Anoshkin IV, Nasibulin AG, Jiang H, Kauppinen EI, Mikoushkin VM, Shnitov VV, Marchenko DE, Noreus D (2011) ACS Nano 5:5132
26. Feng QL, Wu J, Chen GQ, Cui FZ, Kim TN, Kim JO (2000) J Biomed Mater Res 52:662
27. Shvedova AA, Castranova V, Kisin ER, Schwegler-Berry D, Murray AR, Gandelsman VZ, Maynard A, Baron P (2003) J Toxicol Environ Health A 66:1909